Lira-Junior *et al. Genome Medicine* (2026) 18:74
https://doi.org/10.1186/s13073-026-01677-z

Genome Medicine

RESEARCH Open Access

Systemic multi-omics analysis reveals interferon response heterogeneity and links lipid metabolism to immune alterations in severe COVID-19

Ronaldo Lira-Junior[1†], Anoop T. Ambikan[2†], Axel Cederholm[3†], Sefanit Rezene[2†], Flora Mikaeloff[2], Sara Svensson Akusjärvi[2], Ahmet Yalcinkaya[3], Xi Chen[2], Maike Sperk[2], Maribel Aranda-Guillén[4], Hampus Nordqvist[5], Carl Johan Treutiger[5,6], Nils Landegren[3,4], Ujjwal Neogi[2] and Soham Gupta[2*]

Abstract

Background Interferons play a central role in antiviral defense, but their dysregulation contributes to inflammation and immune dysfunction in respiratory viral infections, including COVID-19. While interferon-stimulated genes (ISGs) are essential effectors of this response, their expression patterns in patients are heterogeneous and not always predictive of disease severity. The immunometabolic consequences of this heterogeneity remain poorly understood.

Methods We analyzed hospitalized COVID-19 patients ($n = 37$) and uninfected controls ($n = 31$) using whole-blood transcriptomics, immune cell deconvolution, plasma proteomics, and standardized plasma metabolomics from a previously generated dataset within this cohort. Patients were stratified into low (LIS), moderate (MIS), and high (HIS) ISG score clusters. Plasma innate immune activation markers were measured by ELISA. Interferon-directed antibody reactivity was analyzed by multiplex bead-based assays measuring antigen reactivity. Functional immune responses were assessed via ex vivo stimulation of healthy donor immune cells with patient plasma, and correlations were performed between metabolites and immune activation markers.

Results HIS patients exhibited increased inflammatory mediators and innate immune cell expansion compared with LIS and MIS groups. However, within the HIS group, severe cases displayed distinct metabolic and immune dysregulation. Specifically, severe HIS cases showed reductions in phospholipids, sphingolipids, and tricarboxylic acid cycle intermediates, suggestive of disrupted mitochondrial and lipid metabolism. Plasma from severe HIS patients tended to impair neutrophil and monocyte activation, indicating functional attenuation of innate immune activation within a shared high-ISG background. Correlation analysis revealed that branched-chain lipids, tryptophan-derived metabolites, and a branched-chain dicarboxylic acid were positively associated with immune activation markers.

†Ronaldo Lira-Junior, Anoop T. Ambikan, Axel Cederholm and Sefanit Rezene contributed equally as first authors.

*Correspondence:
Soham Gupta
soham.gupta@ki.se

Full list of author information is available at the end of the article

Although type-I interferon neutralization was detected in a subset of patients with IFN antigen reactivity, these samples did not fully account for the observed ISG heterogeneity or disease severity.

Conclusions High ISG expression in COVID-19 defines a transcriptional endotype associated with systemic inflammation and innate immune activation. However, severe cases within this group exhibit metabolic constraints and reduced innate immune responsiveness, supporting an immune-metabolic axis in which inflammatory mediators and altered lipid/energy metabolism intersect with innate immune function. These findings motivate future studies to determine whether interferon-associated immune-metabolic states during acute infection relate to persistent inflammation or post-acute sequelae in selected patient subsets.

Keywords Interferon-stimulated genes (ISGs), Type I interferons, Immune-metabolic dysregulation, COVID-19, Neutrophil activation, Interferon autoantibody, Metabolic changes

Background

The coronavirus disease 2019 (COVID-19) is caused by the severe acute respiratory syndrome coronavirus 2 (SARS-CoV-2) which exhibits a wide range of clinical manifestations, from asymptomatic infection to severe respiratory distress with systemic complications [1]. A key feature of severe infection is hyperinflammation driven by dysregulated immune signaling caused by proinflammatory cytokines, including alterations in interferon (IFN) responses [2]. Interferons (IFN) are specialized type of cytokines that mediate antiviral defense upon viral RNA recognition by receptors such as RIG-I or MDA-5 receptors [3]. IFNs induce the interferon-stimulated genes (ISGs) through a signaling cascade, activating three major IFN-classes: type I IFN (IFN-α, -ß, -ε, -κ, -ω), type II (IFN-γ), and type III (IFN-λ) [4]. While these IFNs signal through distinct receptors, they share downstream ISG activation, with significant overlap between type I and type III IFN responses [5, 6].

IFNs are among the earliest antiviral responses, with an early and robust response being critical for effective viral clearance and protection against SARS-CoV-2 infection [7]. However, genetic defects and presence of specific IFN-blocking autoantibodies can dampen their antiviral role and cause an inability to control SARS-CoV-2 replication, leading to a more severe disease [8, 9]. While some studies report a suppressed IFN-response in severe cases [10], others describe an elevated ISG expression with heightened inflammation, which correlates with worse disease outcomes [11]. SARS-CoV-2 is known to actively disrupt innate immune responses, contributing to dysregulated IFN signaling [12]. In murine models of human coronavirus infection, a delayed type I IFN response has been linked to excessive monocyte and macrophage activation, driving proinflammatory cytokine storms [4]. Beyond the immune response, metabolic alterations have emerged as critical determinants of COVID-19 severity. IFN signaling can influence lipid metabolism, glycolysis, and amino acid pathways [13]. These metabolic shifts can, in turn, modulate immune cell function and inflammatory outcomes [13]. Furthermore, the dysregulation in IFN response can induce both autoimmune and non-autoimmune inflammatory responses [14]. Autoantibodies against type I IFNs have been implicated in modifying IFN signaling in a subset of patients, although their precise role in disease progression remains complex and context-dependent [9, 15]. Thus, the efficient viral clearance and disease outcome hangs in a balance between IFN response and inflammation. There is considerable multifariousness in the IFN-response and understanding both the protective and aberrant responses can aid in the development of immunomodulatory therapeutic strategies.

Beyond acute infection, IFN response heterogeneity extends beyond COVID-19 severity, influencing post-viral immune dysregulation, persistent inflammation, and metabolic dysfunction. Emerging evidence suggests that dysregulated ISG expression may contribute to post-viral syndromes such as long COVID, where prolonged immune activation and metabolic shifts are implicated in sustained fatigue, neurological symptoms, and cardiovascular complications [16]. Additionally, IFN-driven metabolic reprogramming, particularly disruptions in lipid and amino acid metabolism, may underlie broader immune dysfunctions, including autoimmune-like sequelae [17]. Understanding the interplay between IFN signaling, immune metabolism, and inflammatory resolution is therefore critical not only for COVID-19 but also for broader applications in chronic inflammatory and post-viral syndromes.

In this study, we investigate biological perturbations associated with ISG expression patterns in COVID-19 patients, stratifying individuals based on ISG-driven clustering (low-ISG score: LIS, moderate-ISG score: MIS, and high-ISG score: HIS). Using multi-omics data (plasma proteomics and metabolomics), IFN antigen-reactivity screening, and immune activation analyses, we explore how IFN response heterogeneity is linked to immune and metabolic alterations. Our findings reveal a stochastic relationship between ISG expression and immune cell activation, along with significant perturbations in lipid and amino acid metabolism. These insights

offer a framework for understanding the complex interplay between IFN signaling, immune responses, and metabolic adaptation in COVID-19, which could aid in personalized treatment strategies.

Methods

Study design and patients

The study included both peripheral blood mononuclear cells (PBMCs) and plasma from SARS-CoV-2 infected individuals with available whole-blood transcriptomics data (n = 37) hospitalized in Stockholm, Sweden during May 2020. These individuals were separated into the category of mild (n = 26) or severe (n = 11) disease based on O_2 requirement (O_2 consumption < 4 L/min and > 4 L/min for mild and severe respectively). The cohort was further complemented with non-infected individuals (n = 31), which were divided into convalescent individuals after SARS-CoV-2 infection (n = 10) and non-infected healthy controls (n = 21). The clinical and demographic parameters of the cohort are as earlier described [18, 19]. The study was approved by the Swedish Ethical Review Authority (Dnr 2020–01865). All individuals gave informed consent, and the study was conducted according to the Declaration of Helsinki.

Measurement of plasma IFN levels

Plasma samples were used to measure the levels of IFNs using LEGENDplex Human type 1/2/3 interferon panel (BioLegend #740396), measuring concentrations of IFN-α2, -β, -γ, -λ1, and -λ2/3. The assay was performed according to the manufacturers' protocol. Samples were acquired on Fortessa (BD Biosciences), and analysis performed in FlowJo 10.8.1 (TreeStar Inc). For analysis samples below the background detection were set to 0 and results reported as the median fluorescence intensity (MFI).

Measurement of plasma cellular activation markers

Plasma levels of neopterin (Tecan, Cat# RE59321) and S100A8/A9 (alarmin/calprotectin) in plasma were measured using enzyme-linked immunosorbent assay (DuoSet ELISA, R&D Systems, USA; cat number DY8226-05), according to the manufacturer's instructions. Circulating neutrophil extracellular traps (NETs) were measured using an myeloperoxidase (MPO)-DNA ELISA, with slight modifications from previous descriptions [20, 21]. An anti-MPO antibody (4 µg/mL; clone 4A4, Bio-Rad Laboratories, USA) was used as capture antibody and an anti-dsDNA antibody from the Cell Death Detection ELISA kit (Roche Diagnostic, Switzerland) was used for detection. Plasma was used at 1:10 dilution in 1% bovine serum albumin (BSA)/phosphate-buffered saline (PBS) and incubated for 2 h at room temperature. The development was done with 3,3', 5,5' tetramethylbenzidine (TMB; BD Biosciences, USA), and the reaction stopped with a 2 N sulfuric acid solution. Absorbance was measured at 450 nm and wavelength correction at 540 nm to subtract background using a microplate reader (SpectraMAX 340, USA).

SARS-CoV-2 antibody and IFN antigen-reactivity screening

Plasma samples were analyzed for antibody reactivity against a panel of recombinant protein antigens using a broad multiplex bead-based array, as described previously [22]. The antigen panel included type I, type II, and type III interferons/cytokines: IFNA1, IFNA2, IFNA4, IFNA5, IFNA6, IFNA7, IFNA8, IFNA10, IFNA14, IFNA16, IFNA17, IFNA21, IFNB1, IFNE, IFNG, IFNK, IFNL4, IFNW1, IL28A, IL28B, IL29, GM-CSF, IL1F6, IL1RN, IL12, IL17A, IL17F, IL22, IL23, and ISG15. Antibody reactivity against SARS-CoV-2 spike S1/S2, receptor-binding domain (RBD), nucleocapsid, and Epstein-Barr virus EBNA1 was also assessed.

Briefly, recombinant proteins were coupled to magnetic beads (MagPlex®, Luminex Corp., Austin, Texas) using AnteoTech Activation kit for Multiplex Microspheres (Cat# A-LMPAKMM-10) with commercial versions of the proteins (1.5×10^6 beads were coupled using 3 µg of proteins). One microliter of sample was diluted 1:25 in PBS and later diluted 1:10 in 0.05% PBS with 3% BSA and 5% Milk. The sample dilution was subsequently incubated for two hours with 5 µL of the bead solution on a 650 rpm shaker. After three washings in 0.05% PBS, beads were resuspended in 50 µL of 0.2% PFA during 10 min. The secondary antibody (Invitrogen, H10104 lot#2,384,336) incubation lasted for 30 min prior to the final analysis in FlexMap 3D instrument (Luminex Corp). For each sample-antigen pair, antibody binding was quantified as the mean fluorescence intensity (MFI), calculated from multiple beads coupled to the same antigen. A cutoff for positivity was defined for each antigen as the mean MFI of the healthy control group + 7 SD.

Neutralization analysis for type I IFN autoantibodies

Neutralization assays were performed on samples identified for further analysis based on high ISG scores or elevated responses to type-I interferons in a multiplex screening assay (threshold: mean + 7 standard-deviations (SDs)). The assay followed previously reported cell culture-based neutralization protocols [23], utilizing a dual-luciferase reporter system in HEK293T cells to assess the functional inhibition of interferon signaling. On day 1, HEK293T cells in logarithmic growth were detached using 0.01% trypsin, washed, and resuspended at 1×10^6 cells/mL in DMEM (Gibco) supplemented with 10% FBS and 100 U/mL penicillin–streptomycin. A total of 35,000 cells per well were plated in a 96-well flat-bottom plate. After 3–4 h of incubation at 37 °C to

allow for attachment, cells were transfected using Firefly pGL4.45[luc2P/ISRE/Hygro] (IFN-stimulable) and Renilla pRL-SV40 (constitutive control) vectors (Promega) with X-tremeGENE9 transfection reagent (Sigma-Aldrich) at a 3:1 ratio (µL:µg) in OptiMEM medium. The final transfection mix contained 0.8 µg Firefly and 0.4 µg Renilla plasmid per well. Transfection controls were included, and plates were incubated at 37 °C for 24 h. On day 2, stimulation was initiated by adding 5 µL of IFN-α2 (100 ng/mL, MedChemExpress) to achieve a final concentration of 10 ng/mL per well, followed immediately by 5 µL of plasma samples (1:10 final dilution in a total 50 µL volume). Non-stimulation controls received media instead of IFN-α2, and non-plasma technical controls received media instead of plasma. Positive control samples from APS1 patients (known neutralizing autoantibodies) and negative control blood donor plasma were included. On day 3, following 24 h of incubation, neutralization was assessed using the Dual-Luciferase Reporter Assay System (Promega). Cells were lysed, and luminescence was measured using a plate reader (Tecan, Magellan) with Firefly (magenta filter) and Renilla (green filter) detection. The Firefly-to-Renilla ratio was calculated, with Renilla readings serving as internal controls to correct for variations in transfection efficiency and cell viability. APS1 patient samples exhibited complete neutralization (> 99%, Firefly/Renilla ratio < 0.050), while healthy donor samples showed no neutralization (> 2.000 ratio). A standard response curve was generated using APS1 samples (0% response) and blood donors (100% response). Definite neutralization was defined as > 90% response reduction, while partial neutralization was categorized as 80–90% response reduction. The assay controls performed as expected, confirming the robustness of the neutralization assessment.

Data and preprocessing

Count tables for transcriptomics, olink proteomics data and metabolomics data were retrieved and reanalyzed from Ambikan et al. 2022 [18]. Before analysis, transcriptomics data were filtered for low variance (variance < 0.2) and transformed using variance-stabilizing transformation (VST) from R package DESeq2 v 1.44.0 [24]. Genes expression profile associated with the Reactome (https://reactome.org) pathways antiviral mechanisms, interferon alpha/beta and interferon gamma were extracted from the data. ISG scores were calculated for each patient by making the sum of Z-scaled expression values of genes linked to each pathway [25]. Plasma metabolomics data were derived from a previously published dataset generated from the same cohort and reanalyzed here in the context of ISG-defined stratification [19]. Metabolomics data were $\log_2$-transformed before analysis. The data were obtained from standardized metabolomics platform which enables consistent metabolite annotation and cross-sample comparison but limits direct feature-level matching with discovery-based mass spectrometry datasets commonly used in public COVID-19 cohorts.

Statistics

Spearman pairwise correlations between features were done using the R package Psych v 2.6.3. R package limma v 3.60.6 for differential abundance analysis was used in metabolomics and proteomics data [26] with adjustment for age, gender and BMI category. R package DESeq2 was used to perform differential gene expression analysis in transcriptomics data [24]. Factors of possible unwanted variation in the data estimated using R package RUVSeq v 1.38.0 [27] were adjusted along with age, gender and BMI category while executing DESeq2. Means of continuous variables were compared using Mann–Whitney U test. All *p*-values were adjusted using false discovery rate (FDR) and by default FDR < 0.05 was considered significant. Different cutoffs are indicated in the analysis. Absolute fold change higher than 1 was used as a supplementary cutoff in transcriptomics data.

Cell profiling using digital cell quantification

Digital cell quantification (DCQ) was performed to estimate immune cell proportions from bulk RNA sequencing data using the EPIC deconvolution algorithm [28] with a reference signature of 18 blood cell types from the Human Protein Atlas [29]. Transcripts per million (TPM) normalized gene expression data was used for the analysis. The deconvolution approach utilized a constrained least-squares regression to infer relative immune cell proportions based on predefined reference profiles. To assess the relationship between interferon-stimulated gene (ISG) expression and immune cell distributions, DCQ-derived cell fractions were correlated with ISG scores using Spearman's rank correlation with false discovery rate (FDR) correction for multiple comparisons. All statistical analyses were conducted using R (v 4.4.1), with significance thresholds set at FDR < 0.05 unless otherwise specified.

Clustering

Patient clustering was performed based on interferon-stimulated gene profiles from transcriptomics data using R package ConsensusClusterPlus v 1.68.0 [30]. From 2 to 10 clusters were tested (maxK) on 1000 subsamples (reps), with 0.8 of items (pItem) and all features (pFeature) to sample. The clustering algorithm used was hierarchical clustering (hclust). The number of clusters was determined based on Consensus Cumulative Distribution Function (CDF) and delta area plots.

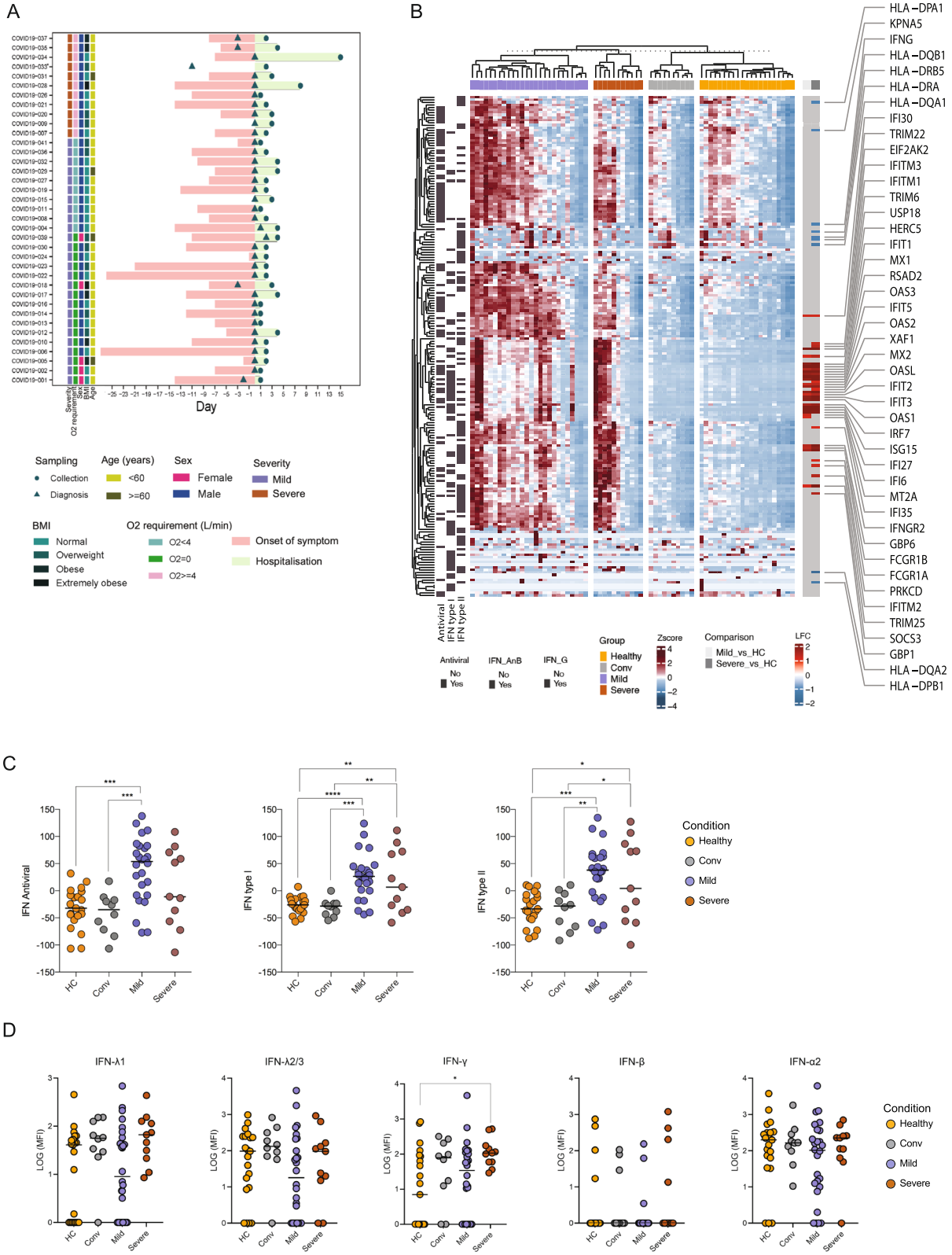

Fig. 1 (See legend on next page.)

(See figure on previous page.)

Fig. 1 Transcriptomic and plasma IFN analysis of COVID-negative healthy controls (HC; $n = 21$), convalescent individuals (Conv; $n = 10$), mild COVID-19 patients ($n = 26$), and severe COVID-19 patients ($n = 11$). **A** Schematic figure showing the clinical characteristics of COVID-19-infected individuals included in the transcriptomic analysis. **B** Heatmap of the interferon-stimulated gene (ISG) profile of the clinical cohort from transcriptomic data. **C** Dot plots of the ISG score for type I ISGs, type II ISGs, and antiviral ISGs in the clinical groups separately. **D** Plasma levels of IFN-λ1, IFN-λ2/3, IFN-γ, IFN-β, and IFN-α2 measured by LEGENDplex assay in the same cohort and expressed as median fluorescence intensity (MFI). Statistical significance was measured using Kruskal–Wallis with false discovery rate (FDR) correction, with significance indicated as $*p < 0.05$, $**p < 0.01$, $***p < 0.001$, and $****p < 0.0001$

Visualisation

Scatter plots, box plots, bubble plots, dot plots, bar plots, principal component analysis (PCA) plots and volcano plots were done using R packages ggplot2 v 4.0.3 and ggpubr v 0.6.3. Heatmaps were done using R package ComplexHeatmap v 2.20.0.

Plasma treatment of neutrophils and PBMCs for monocyte activation and flow cytometry analysis

Neutrophils and PBMCs were isolated from buffy-coated blood of healthy donors using density gradient centrifugation with Ficoll-Paque PLUS (GE Healthcare). Whole blood was diluted 1:1 with PBS, layered over Ficoll, and centrifuged at 400 × g for 30 min at room temperature without brake. The PBMC layer was collected, washed twice in PBS, and resuspended in RPMI-1640 (Gibco) supplemented with 2 mM L-glutamine and 1% penicillin–streptomycin. Neutrophils were isolated from the erythrocyte pellet via hypotonic lysis, followed by washing and resuspension in RPMI-1640 with 2 mM L-glutamine and 1% penicillin–streptomycin.

PBMCs were seeded in 96-well U-bottom plates at 2×10^5 cells/well, and neutrophils were plated in 96-well flat-bottom plates at 2×10^5 cells/well. Cells were treated with 10% plasma (1:10 dilution in culture medium) from COVID-19 patients stratified by disease severity (mild vs. severe) within the high ISG expression (HIS) group. Control wells received plasma from healthy blood donors (negative control). PBMCs were incubated for 24 h and neutrophils for 4 h at 37 °C with 5% CO2.

Following incubation, cells were washed and stained with fluorophore-conjugated antibodies for activation markers. PBMCs were stained for monocyte activation using CD169 (Siglec-1, clone 7–239, BV421; BD Biosciences), a marker induced by type-I IFNs, along with CD14 (clone M5E2, PerCP; BioLegend) and HLA-DR (clone L243, PE/Cy7; BioLegend) for monocyte gating. Neutrophil activation was assessed using CD11b (clone ICRF44, PE; BioLegend), CD66b (clone G10F5, FITC; BioLegend) and CD62L (clone DREG-56, BV421; BioLegend). A viability dye (Live/Dead Fixable, Thermo Fisher) was used to exclude dead cells. Samples were acquired on a BD FACSVerse flow cytometer, and data were analyzed using FlowJo v10.

Mean fluorescence intensity (MFI) values for CD169, CD11b, CD66b, and CD62L were compared between treatment groups using Kruskal–Wallis tests followed by Dunn's post-hoc analysis. Correlations between metabolic alterations and immune activation markers were assessed using Spearman's rank correlation with FDR correction. Statistical analyses were conducted in GraphPad Prism 9 and R v 4.1.0, with significance set at FDR < 0.05 unless otherwise specified.

Results

IFN-signatures in COVID-19 disease severity

Interferons (IFNs) induce interferon-stimulated genes (ISGs) with antiviral functions, and dysregulated IFN responses have been linked to COVID-19 severity. Although SARS-CoV-2 primarily infects respiratory tissues, whole-blood profiling captures systemic interferon signaling and circulating immune-metabolic states that may modulate disease course. To investigate the link between IFN-signaling and disease severity, we analysed whole-blood RNA-seq data from 21 COVID-negative healthy controls (HC), 10 convalescent individuals (Conv), 26 mild and 11 severe COVID-19 patients (Fig. 1A) previously described by us [18]. Transcriptomic analyses focused on genes involved in the type I IFN (IFN-α/ß) signaling pathway (R-HSA-909733), type II IFN (IFN-γ) signaling pathway (R-HSA-877300), and antiviral ISG pathway (R-HSA-1169410) (Additional file 1: Table S1), with overlapping ISGs across pathways. Both the mild and severe patient groups showed a significant increase in ISG expression, predominantly within the type I IFN signaling (FDR < 0.05, Fig. 1B). To capture patient-specific IFN responses, we computed ISG scores for type I, type II, and antiviral signaling pathways by summing gene-wise Z-scores within a given pathway [25] (Additional file 2: Table S2). A significant increase in ISG score for all three pathways was observed in mild disease compared to healthy, while no difference was seen between the mild and severe groups (Fig. 1C, Mann Whitney U test, p-value < 0.05). Despite similar aggregate ISG scores, visualization of ISG expression revealed distinct gene expression patterns between mild and severe cases, indicating underlying heterogeneity (Fig. 1B). All the severe cases in our cohort were male and no sex-specific separation of ISG-scores was observed within the mild group.

IFNs activate ISGs via the JAK-STAT pathway. To assess whether ISG expression reflected circulating IFN levels, we examined IFN gene expression and plasma IFN concentrations. At the transcript level, most IFN gene

were expressed at low or undetectable levels (Transcripts per million, TPM < 1), except for *IFNL1* and *IFNG*, showing reduced expression in severe cases (Additional file 3: Fig. S1). Plasma IFN-I (IFN-α2 and IFN-β), IFN-II (IFN-γ), and IFN-III (IFN-λ1 and IFN-λ2/3) were measured using a FACS-based LEGENDplex assay. Due to low concentrations, median fluorescence intensity (MFI) was used for analysis. No significant differences in circulating IFN levels were observed across patient groups (Kruskal–Wallis test, FDR > 0.05, Fig. 1D, Additional file 4: Table S3). However, IFN-γ was higher in severe COVID-19 compared with HC (adjusted $p = 0.042$).

COVID-19 patient stratification based on the ISG expression

ISG expression showed marked heterogeneity between clinical groups. While ISG scores were uniformly distributed among mild cases, severe cases displayed a bimodal distribution, with five patients exhibiting high ISG scores and six showing near-baseline levels (Fig. 1C). This pattern prompted re-categorization of all samples based on their transcriptomic ISG profiles. To address this heterogeneity, we performed a robust hierarchical consensus clustering of the patients based on ISGs expression profile. This approach segregated subjects into three clusters, supported by a consensus matrix and visualized by PCA analysis (Figs. 2A, Additional file 3: Fig. S2). Clusters were defined based on ISG scores across the three IFN pathways and designated as low-ISG score (LIS), moderate-ISG score (MIS), and high-ISG score (HIS), with LIS resembling the healthy control profile (Mann Whitney U test, p-value < 0.05, Fig. 2B-2C). The alignment of these clusters with previous clinical categorizations is displayed in Fig. 2B. Notably, ISG-defined clustering did not fully align with clinical severity. While most mild cases clustered within MIS and HIS, severe cases were distributed across both LIS and HIS (Fig. 2B), indicating that severe COVID-19 can occur in the context of either low or high systemic ISG expression. To assess whether this ISG heterogeneity could also be detected in independent datasets, we applied the same ISG scoring framework to publicly available COVID-19 transcriptomic cohorts, including both bulk RNA-seq and single-cell RNA-seq studies. Across bulk transcriptomic datasets [31, 32], ISG scores displayed broad variability and segregated patients into clusters with distinct interferon transcriptional states, with ISG-high clusters containing both severe and non-severe cases depending on the severity definitions used in each study. Consistent with these observations, analysis of publicly available single-cell RNA-seq datasets [33, 34] focusing on circulating monocytes also revealed distinct clusters with markedly different ISG transcriptional states. Monocyte clusters with high ISG scores contained cells originating from multiple clinical categories (Additional file 3: Fig. S3). This dissociation suggests that ISG magnitude alone is insufficient to explain disease severity and points to the existence of distinct immunological endotypes among hospitalized patients. To explore the biological basis of this heterogeneity, we next examined whether hospitalized patients with severe disease differed depending on their ISG-defined endotype, focusing on systemic inflammation, immune activation, and metabolic perturbations.

IFN antigen reactivity and neutralizing autoantibodies across ISG-defined patient clusters

Inborn errors of IFN immunity and neutralizing autoantibodies against IFNs have been associated with immune dysregulation and severe COVID-19 [8, 9]. To assess whether IFN autoantibodies contributed to ISG-defined heterogeneity, we screened patient plasma using an autoantigen array featuring recombinant type I, II, and type III IFN antigens. Samples exceeding the antigen-specific positivity threshold (mean MFI of healthy controls + 7 SD) were considered reactive and marked with asterisks in Fig. 2D. Samples with IFN antigen reactivity were detected in a small subset of COVID-19 patients across LIS, MIS, and HIS, as well as in a minority of convalescent samples. Most IFN antigen-reactive COVID-19 patients clustered within MIS, with single cases observed in LIS and HIS. Additional reactivities against GM-CSF and IL-12 were also detected (Fig. 2D).

To evaluate the functional impact of IFN-α2, neutralization assays were performed on IFN antigen-reactive samples using a dual-luciferase ISRE reporter system. Four of six tested antigen-reactive samples showed > 80% neutralization capacity, spanning LIS, MIS, and HIS groups (Bottom row, Fig. 2D). Notably, only one neutralizing sample corresponded to a severe HIS case, and one convalescent sample also displayed IFN-neutralizing activity. Importantly, no consistent association was observed between IFN antigen reactivity, ISG-defined clustering, or clinical severity. We additionally assessed antibody reactivity against SARS-CoV-2 antigens. HIS patients showed reduced spike and RBD reactivity compared to LIS and MIS, which more closely resembled convalescent profiles (Fig. 2E). In contrast, nucleocapsid-directed antibody responses were preserved across ISG groups, suggesting its potential to be an effective immunogen with implications for both vaccine design and diagnostics.

Although a subset of patients showed IFN-neutralizing activity, this did not correlate with ISG-defined clustering or disease severity in this cohort. These findings indicate that IFN antigen reactivity does not account for the ISG-associated immune-metabolic endotypes identified here,

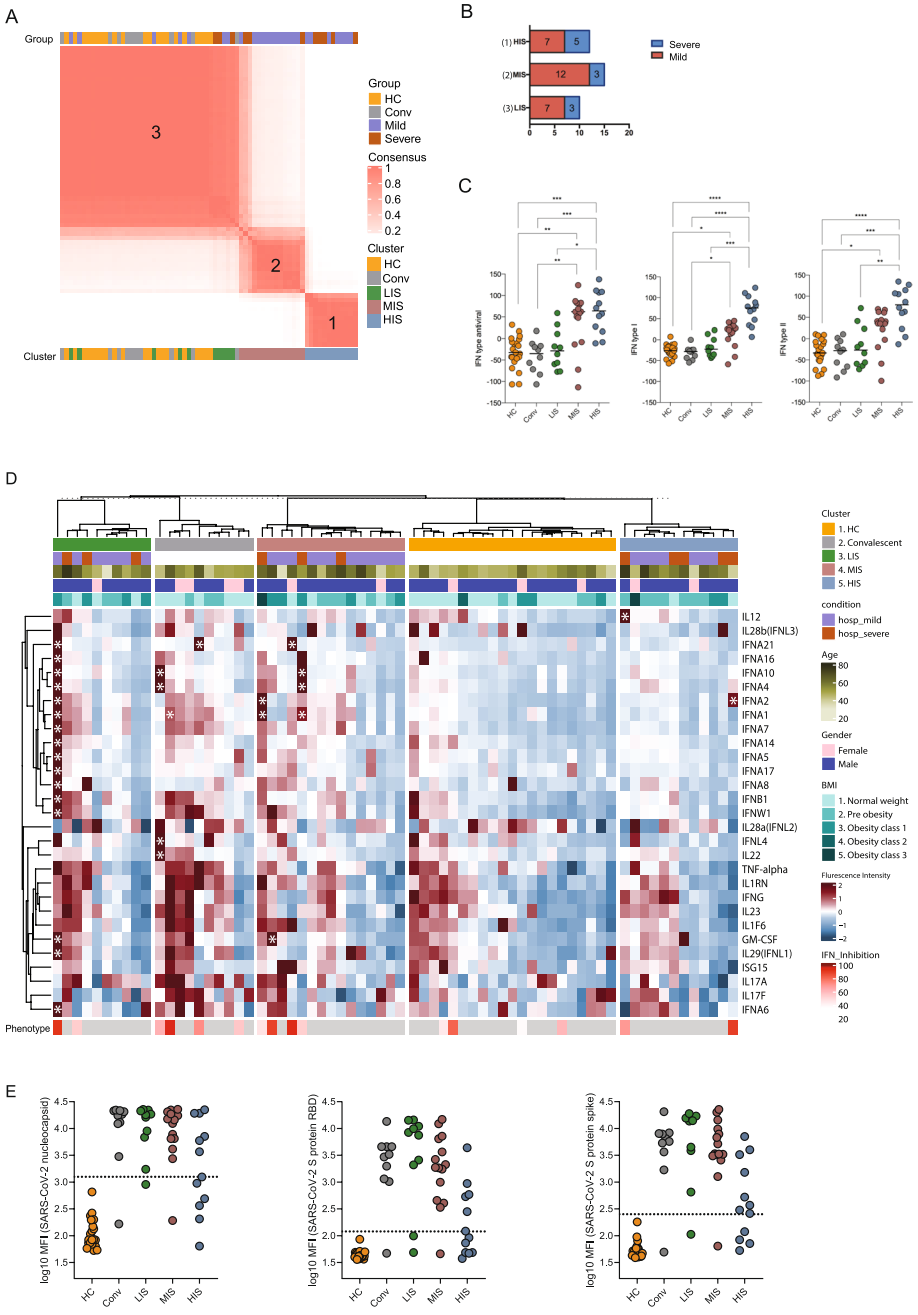

Fig. 2 Clustering of COVID-19 patients based on ISG transcriptomic profiles and detection of IFN reactivities. **A** Heatmap of the consensus clustering matrix depicting patient clustering based on ISG expression. Patients are displayed along both rows and columns, with clinical conditions (top) and ISG-based clusters (bottom) indicated. Consensus values range from 0 (no co-clustering) to 1 (consistent co-clustering) and are color-coded from white to red. Clinical severity (mild/severe) and ISG-defined clusters (LIS/MIS/HIS) represent independent classifications; color coding reflects severity distribution within each cluster. **B** Bar plot showing the distribution of clinically categorized subjects within each ISG-defined cluster: low-ISG score (LIS), moderate-ISG score (MIS), and high-ISG score (HIS). **C** Dot plots illustrating the antiviral, type I IFN, and type II IFN ISG scores across different ISG-defined clusters, highlighting differential ISG expression patterns. Statistical significance was assessed using the Mann–Whitney U test, with significance indicated as $*p < 0.05$, $**p < 0.01$, $***p < 0.001$, and $****p < 0.0001$. **D** Heatmap showing reactivity against recombinant IFN antigens across patient groups and ISG-defined clusters. For each sample-antigen pair, antigen reactivity was assessed by mean fluorescence intensity (MFI), calculated from multiple beads coupled to the same antigen. MFI values were scaled per antigen for visualization. Antigen-reactive samples exceeding the antigen-specific positivity threshold, defined as the mean MFI of healthy controls + 7 SD, are marked with asterisks. The bottom annotation row displays type I IFN neutralization assay results for the corresponding samples where performed. Clinical metadata, including patient condition, ISG-defined cluster, sex, age, and BMI category, are displayed above the heatmap. **E** Dot plots showing antibody reactivity against SARS-CoV-2 nucleocapsid, spike receptor-binding domain (RBD), and spike antigens across ISG-defined clusters. Each point represents one sample, and antibody reactivity is shown as $\log_{10}$-transformed mean fluorescence intensity (log10 MFI). The horizontal dashed line indicates the antigen-specific positivity threshold, defined as the mean MFI of healthy controls + 7 SD

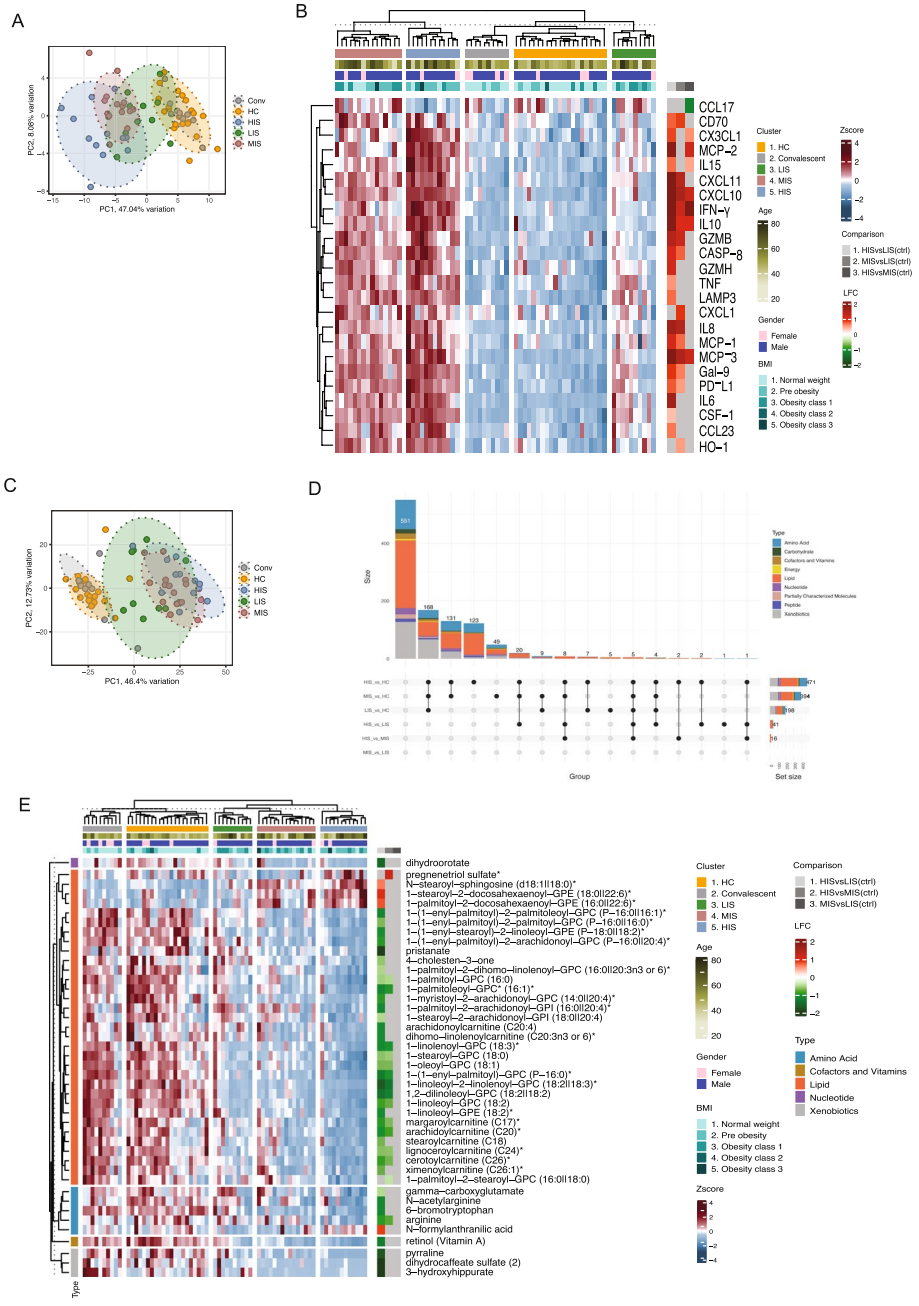

Fig. 3 (See legend on next page.)

but may represent an additional layer of immune dysregulation in a subset of individuals.

Plasma proteomics reveals a progressive increase in inflammation with higher ISG expression

To investigate the relationship between ISG expression and systemic inflammation, we analyzed the plasma inflammatory cytokines measured using Olink immuno-oncology panel [19] across ISG-defined clusters. PCA revealed a clear segregation of samples that mirrored the ISG score-based clustering (Fig. 3A). Healthy controls and convalescents clustered closely, while LIS samples did not form a tight cluster with healthy controls or convalescent individuals, but instead displayed a dispersed distribution spanning the space between HC/Conv and MIS COVID-19 patients. Whereas MIS and HIS samples progressively diverged along PC1 (47.04% variance), indicating an increasing systemic inflammatory burden with higher ISG expression.

To identify specific inflammatory mediators associated with ISG expression, we performed hierarchical clustering using the Olink plasma proteomic data (Fig. 3B).

(See figure on previous page.)

Fig. 3 Multi-omics analysis of inflammatory and metabolic perturbations across ISG-defined clusters. Plasma proteomics and metabolomics data were derived from the previously published dataset in reference [19]. **A** Principal Component Analysis (PCA) plot of Olink proteomic data from healthy controls (HC), convalescent individuals (Conv), and COVID-19 patients stratified into LIS, MIS, and HIS clusters. The first two principal components are displayed, with variance explained indicated on the axes and color-coded cluster categories. **B** Heatmap of significantly differentially expressed plasma proteins across ISG-defined clusters (LIS, MIS, HIS). The main heatmap displays z-score–normalized protein abundance across individual samples, with hierarchical clustering of patients. Columns represent individual samples, rows represent proteins, and hierarchical clustering was applied to samples. Annotation bars on the top of the heatmap indicate ISG cluster, age, sex, and BMI. The adjacent right panel heatmap summarizes $\log_2$ fold changes (LFC) for pairwise cluster comparisons (HIS vs LIS, MIS vs LIS, and HIS vs MIS), indicating the direction and magnitude of differential protein abundance between ISG-defined groups. **C** PCA plot of metabolomic data from HC, Conv, and COVID-19 patients categorized into LIS, MIS, and HIS clusters. The first two principal components are shown, color-coded by cluster categories, highlighting metabolic differences across groups. **D** UpSet plot depicting the overlap of significantly altered metabolites across ISG-defined clusters (LIS, MIS, HIS). The number of differentially abundant metabolites (LIMMA, FDR < 0.05) in each comparison is indicated, highlighting shared and unique metabolic disruptions across clusters. **E** Heatmap of significantly altered plasma metabolites across ISG-defined clusters. The main heatmap displays z-score normalized metabolite abundance across individual samples, within LIS, MIS, and HIS clusters. Metabolite abundance is $\log_2$ transformed and z-score normalized, with hierarchical clustering applied. Row annotation represents indicated metabolites and their super-pathways, while column annotations indicate individual samples within specific ISG clusters. Annotation bars on the top of the heatmap indicate ISG cluster, age, sex, and BMI. The adjacent right panel heatmap summarizes LFC for pairwise cluster comparisons (HIS vs LIS, MIS vs LIS, and HIS vs MIS), indicating the direction and magnitude of metabolic differences between ISG-defined clusters

Hierarchical clustering revealed distinct inflammatory signatures across ISG clusters, characterized by a progressive increase in inflammatory mediators from LIS to HIS (Fig. 3B). Several key inflammatory mediators, including CXCL10, CXCL11, MCP-2, MCP-3, IFN-γ, IL-10, and TNF, showed a graded increase and were significantly elevated in HIS compared to LIS (LIMMA, FDR < 0.05, Additional file 5: Table S4), consistent with chemokine-driven inflammatory program associated with interferon signaling. IL-6 and TNF, both implicated in severe inflammatory responses, were particularly upregulated in HIS, suggesting a potential contribution to disease severity within this ISG-defined group.

Enhanced type I and type II ISG expression in COVID-19 patients reshapes lipid and amino acid metabolism

Increasing evidence supports a close crosstalk between cellular metabolism and IFN-signaling during viral infection. Type I IFN has been shown to modulate glycolysis, lipid metabolism, and oxidative phosphorylation in multiple immune cell types [13]. ISGs induced by IFNs also regulate central carbon metabolism [35]. To examine how IFN-driven transcriptional programs relate to systemic metabolism during COVID-19, we analyzed the ISGs cluster-specific changes in global plasma metabolomics data [19]. Principal Component Analysis (PCA) of metabolomics revealed clustering patterns that closely resembled ISG-defined groups (Fig. 3C). LIS samples clustered near HC and convalescent samples, whereas MIS and HIS samples showed a progressive divergence, with HIS exhibiting the greatest metabolic shift, indicating increasing metabolic dysregulation with higher ISG expression. UpSet analysis identified the highest number of differentially altered metabolites in the HIS vs. LIS comparison (LIMMA, FDR < 0.05; Additional file 6: Table S5), followed by HIS vs. MIS and MIS vs. LIS (Fig. 3D), consistent with a graded metabolic shift across ISG clusters.

Lipid metabolism was the most profoundly affected pathway, followed by amino acid metabolism. Multiple lipid species, including several phospholipids, sphingolipids, and carnitines, were significantly reduced in HIS compared to LIS and MIS (Fig. 3E), suggesting impaired lipid homeostasis. Amino acids such as arginine, gamma-carboxyglutamate, and 6-bromotryptophan were also reduced in HIS, indicating broader metabolic disruption. Both type I and type II ISG scores showed predominantly a negative association with lipid and amino acid metabolites (Spearman correlation, p-value < 0.05, Additional file 7: Table S6), indicating that heightened interferon-associated inflammation is linked to systemic metabolic depletion. Such metabolic alterations may impair immune cell function, as arginine depletion is associated with T cell dysfunction [36] and tryptophan metabolism plays a key role in immunoregulation [37].

ISG expression is associated with myeloid cell expansion and enhanced inflammatory activation

To relate systemic ISG expression to immune compartment shifts, we inferred immune cell proportions using digital cell quantification (DCQ) based on reference signature of 18 blood cell types from the Human Protein Atlas [29] and the EPIC deconvolution algorithm [28]. Here cell-type estimates were interpreted qualitatively, as relative indicators of immune compartment shifts rather than absolute immune cell frequencies, given the known limitations of whole-blood deconvolution in inflammatory states. DCQ revealed a progressive shift toward an innate immune-dominant state with increasing ISG expression. LIS patients exhibited immune profiles similar to healthy controls, whereas MIS and HIS displayed marked enrichment of innate immune cells, particularly neutrophils and classical monocytes (Fig. 4A, Additional file 3: Fig. S4, Additional file 8: Table S7). Targeted phenotyping in a subset of samples supported these findings, showing increased immature neutrophils in HIS and

higher classical monocytes in both HIS and MIS (not statistically significant), reinforcing the association between ISG expression and inflammatory myeloid cell expansion (Additional file 3: Fig. S5).

To determine whether these expanded innate immune populations were also functionally activated, we measured plasma levels of S100A8/A9 and neopterin, markers of neutrophil and monocyte activation. Both markers were significantly elevated in MIS and HIS compared to LIS (Fig. 4B-C; Mann–Whitney U test, p-value < 0.05, Additional file 9: Table S8), indicating enhanced myeloid activation with increasing ISG expression.

Neutrophil activation can also lead to the formation of NETs, which interact with cytosolic DNA sensors such as cGAS and activate IFN pathways via cGAS-STING signaling [38]. To assess NET formation, we measured MPO:DNA complexes. MPO:DNA levels were significantly increased in MIS, but not in HIS (Fig. 4D), indicating that NETosis is not a defining feature of the ISG-high phenotype. Stratification by disease severity showed that S100A8/A9 and neopterin were elevated in both mild and severe cases, whereas MPO:DNA levels did not differ by severity (Additional file 3: Fig. S6). These findings indicate that NET-associated inflammation represents a distinct immune activation program that is separable from the ISG-high endotype and does not drive severity within the HIS group.

Correlation analysis revealed that LIS showed positive associations with classical monocytes across all ISG pathways, while MIS correlated with additional immune subsets (Fig. 4E; Spearman correlation, FDR < 0.05, Additional file 10: Table S9). Notably, no immune cell type showed a significant positive correlation with ISG scores within HIS, suggesting a more complex immune configuration rather than expansion of discrete cell populations.

Together, these findings indicate that high ISG expression is associated with a systemic innate immune-activated state characterized by relative myeloid enrichment and elevated inflammatory mediators. However, the absence of strong correlations between ISG scores and specific immune subsets within HIS suggests immune dysregulation rather than simple cell expansion. Because HIS includes both mild and severe cases, ISG expression alone is insufficient to explain disease severity, motivating further investigation into additional modulatory factors.

Metabolic and immune dysregulation define disease severity in the high ISG-expressing group by altering neutrophil and monocyte activation

Because severe disease was observed in both LIS and HIS, we focused on the HIS group to identify determinants of severity within a shared high-ISG context. This approach allowed us to interrogate factors associated with disease severity beyond the presence of a strong systemic interferon-stimulated gene signature. DCQ analysis showed that HIS patients had increased neutrophil and monocytes proportions and elevated S100A8/A9 and neopterin levels, indicating that innate immune activation is a defining feature of HIS. However, disease severity was not associated with further increases in myeloid expansion. Moreover, no immune cell type correlated positively with ISG scores within HIS, and NETosis was not elevated, suggesting that functional immune alterations and systemic inflammatory or metabolic factors may underlie severity within this group.

To assess immune activation within the HIS endotype, we incubated healthy isolated neutrophils and PBMCs (for monocytes) with plasma from mild and severe cases and measured activation markers by flow cytometry. Functional assays were restricted to plasma from HIS patients to isolate severity-associated effects within a shared high-ISG background and avoid confounding by differences in baseline interferon responsiveness across ISG clusters. Neutrophils activation was assessed using CD66b, CD11b, and CD62L, while monocyte activation was evaluated using CD169 (Siglec-1). Interestingly, plasma from severe cases showed a tendency towards reduced neutrophil activation, characterized by lower CD66b and CD11b expression, and preserved CD62L expression, together with significantly reduced monocyte activation (low CD169; $p < 0.05$) compared to plasma from mild cases (Fig. 5A). Though we observed a clear trend, substantial inter-individual variability was observed, and not all comparisons reached statistical significance. These findings indicate a trend toward functional suppression of innate immune activation by plasma from severe HIS cases, while highlighting heterogeneity within this group.

To identify soluble mediators associated with disease severity in HIS, we compared inflammatory factors (Olink Immuno-oncology panel), between severe and mild cases using LIMMA (Additional file 11: Table S10). MCP-3, HGF, and IL-6 were significantly elevated in severe HIS cases (Fig. 5B, FDR < 0.05). MCP-3 (CCL7) is a key monocyte-recruiting chemokine [39], consistent with monocyte involvement in severe disease, while HGF, a regulator of tissue repair and immune modulation [40], and IL-6, a major pro-inflammatory cytokine [41], have been linked to immune dysregulation and adverse COVID-19 outcomes. These results indicate that severity within HIS is associated with dysregulated inflammatory signaling rather than ISG magnitude alone.

Metabolomic profiling identified 36 significantly altered metabolites between mild and severe cases (Fig. 5C, LIMMA FDR < 0.05, Additional file 12: Table S11), with energy and lipid metabolism being the most dysregulated pathways. Tricarboxylic acid (TCA) cycle intermediates, particularly citrate and aconitate, were

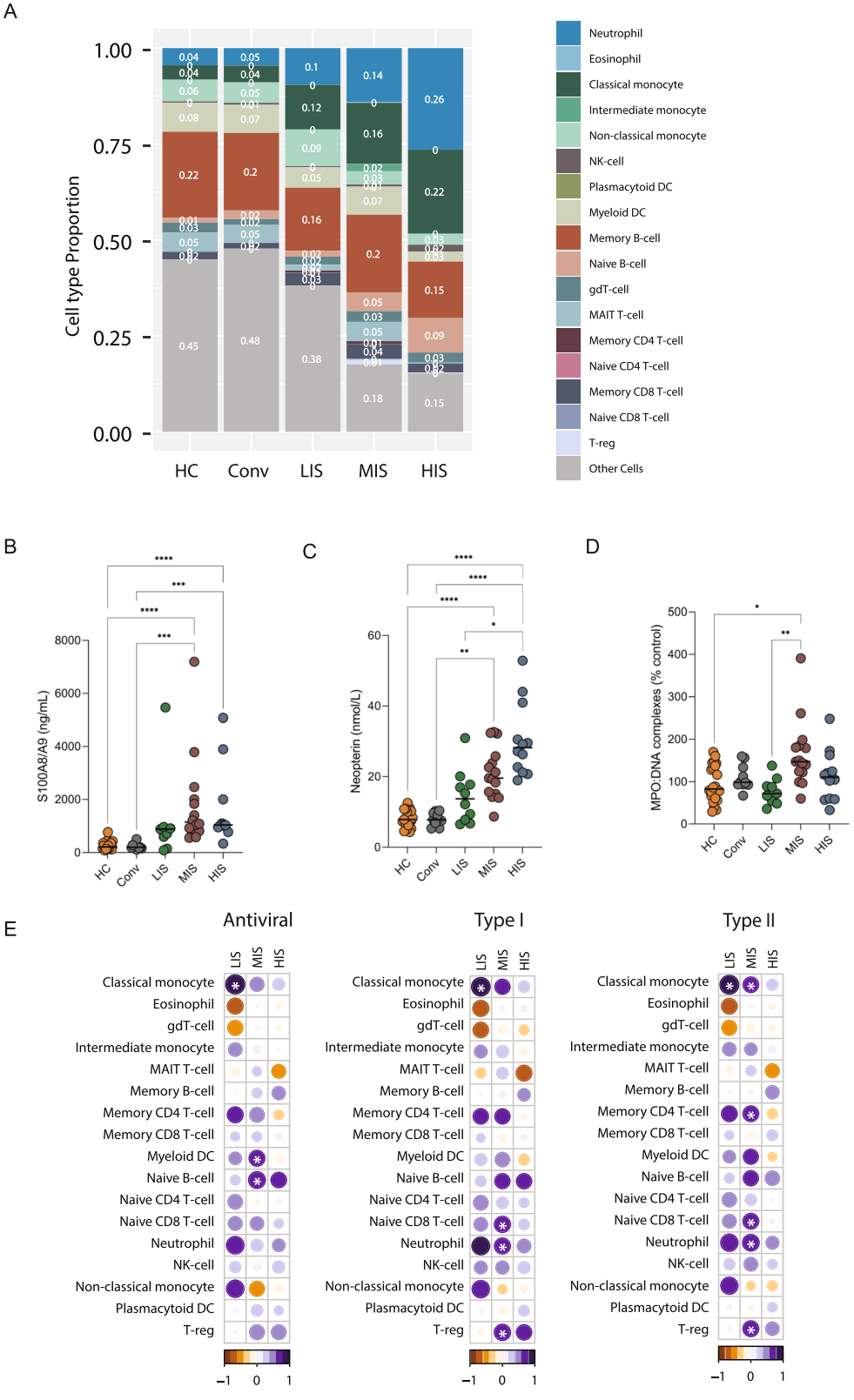

Fig. 4 (See legend on next page.)

(See figure on previous page.)

Fig. 4 Innate immune activation and association with ISG expression in COVID-19 clusters. **A** Stacked bar plot showing the proportion of immune cell types inferred from whole-blood transcriptomics data using reference-based Digital Cell Quantification (DCQ) across healthy controls (HC), convalescent individuals (Conv), and ISG-defined clusters (LIS, MIS, HIS) reflecting relative differences between groups rather than absolute immune cell frequencies. Cell types with a frequency < 0.05 were grouped under "other cells". **B-D** Dot plots depicting plasma levels of key immune activation markers: **B** S100A8/A9 (ng/mL), **C** Neopterin (nMol/mL), and **D** MPO: DNA complexes (% of total), indicative of NETosis, across ISG clusters. *p*-values were calculated using the Mann–Whitney U test, with significance denoted as *$p < 0.05$, **$p < 0.01$, ***$p < 0.001$, and ****$p < 0.0001$. **E** Bubble plot displaying the correlation coefficients between inferred immune cell proportions and ISG expression scores (Left-panel: antiviral; Middle-panel: type I IFN; and Right-panel: type II IFN) within each ISG-defined cluster. Circle color represents the direction of correlation (positive or negative Spearman's rho), while circle size is proportional to the absolute correlation coefficient. Bubbles showing significant correlations (Spearman correlation, $p < 0.05$) are marked with white asterisks highlighting the association between specific immune cell populations and the interferon response

significantly reduced in severe cases, suggesting impaired mitochondrial metabolism which is essential for proper immune activation [42]. Lipid classes such as plasmalogens, phosphatidylcholines, and sphingolipids were also significantly disrupted, potentially affecting membrane integrity, immune signaling, and cell survival [43].

Correlation analysis between significantly altered metabolites and neutrophil/monocyte activation markers (FACS MFI) revealed significant associations for 16 out of 36 significantly altered metabolites with at least one immune activation marker (Fig. 5D; Additional file 13: Table S12, Spearman correlation, *p*-value < 0.05). Several metabolites, including 6-bromotryptophan and branched-chain 14:0 dicarboxylic acid, correlated with both neutrophil (CD11b, CD66b) and monocyte (CD169) activation markers, while others showed stronger associations with monocyte activation. 1,2-dilinoleoyl-GPC (18:2II18:2) correlated with both CD169 and CD11b. Consistent with these findings, key severity-associated inflammatory mediators (MCP-3, HGF, and IL-6) showed predominantly negative correlation trends with multiple metabolites (Additional file 3: Fig. S7), suggesting that heightened inflammatory signaling coincides with systemic metabolic depletion. These findings suggest that metabolic alterations, particularly in tryptophan metabolism, lipid oxidation, and phospholipid remodeling, may influence immune activation and contribute to disease severity within HIS.

In an exploratory analysis of a small subset of patients with available PBMCs, we assessed ISG protein expression by western blot and compared it to transcript levels. In mild cases, ISG15, RIG-I, IRF3, and STING protein levels correlated positively (Spearman's rho > 0.6) with their corresponding transcripts, whereas this relationship was lost in severe cases (Additional file 3: Fig. S8). Although limited by sample size, this observation raises the possibility of post-transcriptional or translational dysregulation contributing to impaired antiviral responses in severe disease.

Discussion

The interferon (IFN)-signaling is activated immediately upon viral infection and plays a pivotal role in antiviral immunity. A balanced IFN response is crucial to eliminating viral infections while preventing excessive inflammation and immune-mediated damage. While timely IFN responses promote viral clearance and are associated with milder COVID-19 outcomes [4, 44], dysregulated or delayed IFN signaling has been implicated in severe disease [8, 9, 45–47]. In particular, excessive or prolonged IFN-associated inflammation, often described as interferonopathy has been linked to immune-mediated tissue damage in critical COVID-19 [48–50]. Together, these observations highlight the dual nature of IFN responses [51, 52] and highlight the need to define when IFN-driven programs are protective versus pathogenic in human disease.

In this study, we identify distinct systemic interferon-associated immune-metabolic endotypes in COVID-19 based on whole-blood interferon-stimulated gene (ISG) expression. While high ISG expression reflects a state of heightened interferon-associated immune activation, our data demonstrate that disease severity emerges only when this transcriptional state coincides with specific inflammatory mediators and metabolic constraints that impair effective innate immune function. This distinction between ISG magnitude and immune functionality provides a framework to reconcile previously conflicting reports on IFN responses in COVID-19 and emphasizes that ISG expression alone is insufficient to predict clinical outcome.

We observed pronounced heterogeneity in systemic ISG expression among COVID-19 patients that was largely independent of disease severity. Severe COVID-19 patients exhibited higher antiviral ISG scores than healthy controls (Fig. 1C), confirming intact induction of interferon-driven antiviral programs at the systemic level. However, the occurrence of severe disease despite robust antiviral ISG expression indicates that IFN-driven transcriptional activation alone does not guarantee protective immunity. Stratification based on whole-blood ISG expression revealed three distinct clusters: low ISG score (LIS), moderate ISG score (MIS), and high ISG score (HIS), each characterized by distinct immune activation state, inflammatory profiles, and metabolic reprogramming. This classification highlights the complex interplay between IFN signaling, innate immune activation,

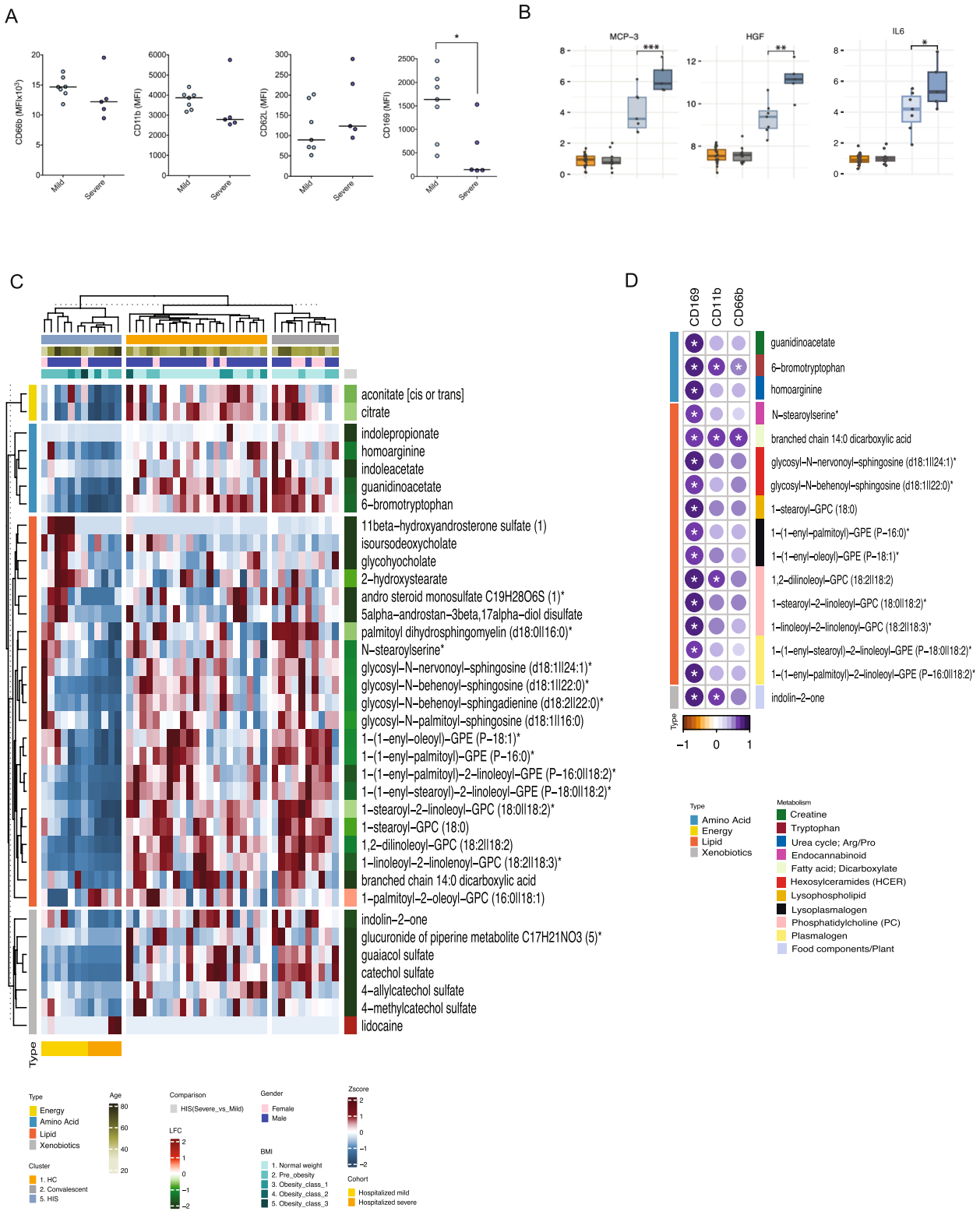

Fig. 5 (See legend on next page.)

(See figure on previous page.)

Fig. 5 Immune and metabolic determinants of severity in the HIS cluster. **A** Dot plots showing the differential ability of plasma from mild and severe HIS cases to activate healthy neutrophils and monocytes in an ex vivo assay. Activation was assessed using CD66b/CD11b for neutrophils and CD169 for monocytes. Lower activation in severe cases suggests the presence of suppressive soluble factors in circulation. Plasma used in the functional assays was derived exclusively from HIS patients and stratified into mild HIS and severe HIS. Healthy donor neutrophils and PBMCs were used as responder cells. **B** Boxplots showing the plasma levels of key inflammatory mediators MCP-3 (CCL7), HGF, and IL-6, in mild (light blue) and severe (dark blue) HIS patients. Severe HIS cases exhibited significantly higher levels of MCP-3, HGF, and IL-6 compared to mild HIS cases. Adjusted *p*-values were calculated using LIMMA, with significance thresholds: $*p < 0.05$, $**p < 0.01$ and $***p < 0.001$. **C** Heatmap of log2-scaled and Z-score transformed metabolite levels significantly altered between mild and severe HIS cases. Xenobiotics were excluded. Rows represent super-pathways of metabolites, and columns represent individual HIS patient samples. **D** Bubble plot showing Spearman correlation coefficients between significantly altered metabolites and neutrophil (CD66b, CD11b) and monocyte (CD169) activation markers in HIS patients. *p*-values < 0.05 were considered statistically significant. Bubble color represents the direction and magnitude of the correlation coefficient, as indicated by the color scale. Bubble size reflects the absolute strength of the correlation (Spearman's rho) with larger bubbles indicating stronger associations. Asterisks denote statistically significant correlations ($p < 0.05$, Spearman's correlation). Only metabolites significantly altered in HIS compared to LIS or MIS (LIMMA, FDR < 0.05) were included

and systemic metabolism during acute SARS-CoV-2 infection.

The distribution of clinical severity across these ISG-defined endotypes further supports a non-linear relationship between interferon responses and disease outcome. Mild cases were enriched within the MIS and HIS groups, whereas severe disease occurred predominantly at the extremes, within both LIS and HIS, with relatively few severe cases in MIS (Fig. 2B). This pattern suggests that intermediate systemic ISG activation may reflect a balanced immune state compatible with antiviral control, while severe disease may arise either in the context of insufficient interferon activity (LIS) or sustained interferon-associated inflammation (HIS). Consistent with this interpretation, independent bulk and single-cell transcriptomic datasets similarly demonstrated heterogeneous ISG transcriptional states, with ISG-high clusters containing samples or cells originating from multiple clinical categories (Additional file 3: Fig. S3), supporting that interferon-associated endotypes are not uniquely defined by disease severity. Supporting this interpretation, principal component analyses of plasma metabolomics and proteomics restricted to severe cases revealed that severe HIS patients segregated from severe LIS and MIS patients despite comparable clinical severity (Additional file 3: Fig. S9), indicating that severe COVID-19 can arise through biologically distinct immune-metabolic trajectories rather than a single severity continuum.

Analysis of circulating interferon transcripts and proteins further clarifies the relationship between interferon signaling and systemic ISG expression. Although low-level IFN mRNA transcripts were detectable in whole-blood RNA sequencing, plasma concentrations of type-I and type-III interferons did not differ consistently across disease severity groups and showed no correlation with ISG scores (Fig. 1D). This uncoupling contrasts with influenza infection, where interferon protein levels closely track antiviral gene expression [53], and is consistent with reports describing temporally dysregulated interferon responses in COVID-19 [10]. Together, these findings indicate that IFN mRNA and protein measurements provide limited explanatory power for systemic ISG heterogeneity and support the interpretation that ISG signatures reflect downstream, context-dependent interferon-associated immune states rather than contemporaneous interferon abundance.

Neutralizing autoantibodies against type I interferons have been implicated in severe COVID-19 by impairing IFNAR signaling and downstream ISG activation [54, 55]. In our cohort, IFN antigen reactivity was detected in a small subset of patients across ISG-defined clusters using a relatively stringent cutoff compared with other studies that have used different approaches [56, 57], with functional neutralization observed in several cases. However, IFN antigen reactivity did not correlate with disease severity, ISG expression levels, or circulating interferon protein abundance. These findings indicate that IFN antigen reactivity does not account for the systemic interferon-associated immune-metabolic endotypes identified in this study and are unlikely to be a primary driver of ISG heterogeneity in this cohort. The detection of IFN antigen reactivity in convalescent plasma further raises questions about the persistence of immune dysregulation beyond acute infection, but larger longitudinal studies will be required to define its clinical relevance.

A defining feature of the HIS endotype was enrichment of innate immune activation, reflected by increased neutrophil and monocyte proportions inferred by DCQ and elevated plasma levels of S100A8/A9 and neopterin, markers of neutrophil and macrophage activation, respectively. Neutrophils are key effectors of innate immunity and express cytosolic pattern-recognition receptors such as RIG-I and MDA5, enabling interferon-associated activation upon viral sensing [58]. Upon activation, neutrophils can release S100A8/A9, an alarmin that functions as a damage-associated molecular pattern to amplify inflammatory signaling and recruit additional immune cells [59]. S100A8/A9 has been implicated in SARS-CoV-2–associated immunopathology [60], and its elevation in MIS and HIS in our cohort supports its role as a marker of interferon-associated myeloid activation

rather than a direct determinant of disease severity. Consistent with this, SARS-CoV-2 infection has been shown to induce alarmin release, promoting expansion and activation of immature neutrophils and contributing to dysregulated innate immune responses [61]. Neopterin, released by activated macrophages upon IFN-γ induction [62], followed a similar pattern, further supporting the role of IFN-driven myeloid cell activation within the HIS cluster. ISGs can be induced through both IFN-dependent JAK-STAT signaling and IFN-independent IRF3 activation [63, 64]. In COVID-19, neutrophil activation has been linked to NET formation [65], which can further amplify interferon signaling via cGAS-STING activation [38]. However, despite previous reports linking NETs to severe COVID-19 [21], our findings did not indicate any association between NET formation and either disease severity or HIS endotype. Instead, NETosis was most prominent in the MIS group, indicating that NET-associated inflammation represents a distinct immune activation program that is separable from the ISG-high systemic state.

Within the HIS endotype, disease severity was associated with a coordinated inflammatory and metabolic state rather than with the magnitude of interferon-stimulated gene expression alone. Severe HIS cases exhibited elevated circulating levels of MCP-3 (CCL7), hepatocyte growth factor (HGF), and IL-6, mediators implicated in monocyte recruitment [39], tissue remodeling, and systemic immune dysregulation in COVID-19 [40, 41]. These inflammatory signals coincided with depletion of TCA cycle intermediates, including citrate and cis-aconitate, and reduced abundance of multiple lipid classes involved in membrane integrity and immunometabolic signaling. Such metabolic perturbations are consistent with impaired mitochondrial function and reduced bioenergetic capacity, conditions known to limit effective innate immune cell activation.

During viral infection, immune cells undergo extensive metabolic reprogramming to meet the energetic and biosynthetic demands of innate immune activation, while viruses can exploit host metabolic pathways to support its own replication [66, 67]. In line with this, our metabolomic profiling revealed significant alterations in amino acid and lipid metabolism, with suppression of TCA cycle emerging as a defining feature of severe disease in HIS endotype. Reduced circulating levels of citrate and aconitate suggest mitochondrial dysfunction, which may impair energy metabolism and immune cell function [42]. In parallel, depletion of lipids such as plasmalogens, phosphatidylcholines, and sphingolipids which are essential for membrane stability, receptor signaling and immune cell communication [43, 68] is consistent with impaired immune signaling and defective inflammatory resolution. These findings are concordant with reports from independent COVID-19 cohorts across different geographical regions, which have described broad perturbations in amino acid and lipid metabolisms in severe or fatal COVID-19 [69]. However, unlike prior studies, our analysis directly links these metabolic alterations to interferon-associated immune states, highlighting a previously underexplored connection between IFN-driven inflammation and systemic metabolic dysfunction.

Experimental models have shown that reduced lipid biosynthesis can itself induce type I IFN responses in a STING dependent manner [70], providing a mechanistic framework that falls in line with our observation of lowered lipid metabolite levels in patients with high ISG expression. Importantly lipid depletion was further associated with the disease severity in both HIS and MIS clusters, with distinct lipid signatures observed in each group, suggesting that interferon-associated metabolic stress represents a broader feature of COVID-19 immunopathology rather than a uniform consequence of disease severity. Notably, reduced levels of citrate and cis-aconitase, central intermediates linking the TCA cycle to fatty acid metabolism were unique to severe HIS cases. Both metabolites support the production of itaconate, a metabolite with well established anti-inflammatory and IFN-regulatory function and its derivatives have inhibitory effects on virus replication, including SARS-CoV-2 [71–73]. Their depletion suggests loss of a key immunoregulatory metabolic axis in severe disease. Correlation analyses linking these metabolic alterations to reduced neutrophil (CD66b, CD11b) and monocyte (CD169) activation further support a model in which metabolic constraints actively limit immune cell responsiveness rather than simply reflecting downstream consequences of inflammation.

Sex is a recognized risk factor for severe COVID-19, with male patients exhibiting higher rates of hospitalization and adverse outcomes [74, 75]. In our cohort, all severe cases were male, limiting our ability to disentangle sex-specific effects from disease severity. However, comparison of ISG scores between male and female patients revealed no significant differences across antiviral, type I IFN-associated, or type II IFN-associated ISG signatures (Additional file 3: Fig. S10). These findings suggest that sex-associated risk is unlikely to be mediated by differences in systemic ISG induction and may instead reflect downstream differences in immune regulation, metabolic resilience, or tissue-specific immune responses not captured here. Larger, sex-balanced cohorts will be required to resolve these mechanisms.

Our study has several limitations. First, metabolic alterations were assessed in plasma, precluding direct

conclusions about intracellular metabolic changes in immune cells. Second, while significant associations between metabolic changes and immune activation were observed, causal relationships remain to be established. Third, reliance on whole-blood bulk transcriptomics limits its assignment of ISG expression to specific cell types, and digital cell quantification was therefore interpreted qualitatively. Fourth, COVID-19 immunopathology is highly compartmentalized, and peripheral blood analyses may not fully capture tissue-resident immune responses in organs such as the lung or kidney. Our analyses are limited to peripheral blood defining systemic immune-metabolic states reflected in circulation and therefore do not directly capture tissue-resident immune cell programs or local antiviral responses. Finally, the absence of disease or vaccination controls and the modest cohort size limit generalizability. Although this cohort derives from the first pandemic wave, the host response pathways interrogated here including interferon signaling, innate immune activation, and immunometabolic regulation represent fundamental biological processes that are unlikely to be variant-specific. External validation of these immune-metabolic endotypes is currently constrained by the lack of harmonized patient-level datasets integrating bulk transcriptomics, broad plasma metabolomics, and immune activation phenotyping with comparable severity metadata.

Conclusions

Our findings demonstrate that systemic ISG expression delineates distinct immune-metabolic endotypes in COVID-19, but ISG magnitude alone does not determine disease severity. Instead, severity emerges from the convergence of interferon-associated inflammation with metabolic constraints that impair effective innate immune function. These results position immunometabolism as a central determinant of disease outcome and suggest that therapeutic strategies aimed at restoring metabolic homeostasis such as modulation of lipid metabolism or replenishment of TCA cycle intermediates may enhance immune competence in selected patient subsets. More broadly, understanding how IFN-driven immune programs intersect with metabolism may inform precision approaches to viral infections and inflammatory diseases beyond COVID-19.

Abbreviations

BSA	Bovine serum albumin
CDF	Consensus cumulative distribution function
Conv	Convalescent group
COVID-19	Coronavirus disease 2019
DCQ	Digital cell quantification
FDR	False discovery rate
HC	COVID-negative control
HGF	Hepatocyte growth factor
HIS	High-ISG score
IFN	Interferon
ISG	Interferon-stimulated gene
LFC	Log_2 fold changes
LIS	Low-ISG score
MIS	Moderate-ISG score
MPO	Myeloperoxidase
NETs	Neutrophil extracellular traps
PBMCs	Peripheral blood mononuclear cells
PBS	Phosphate-buffered saline
PCA	Principal component analysis
RBD	Receptor-binding domain
SARS-CoV-2	Severe acute respiratory syndrome coronavirus 2
SD	Standard deviation
TMB	3,3', 5,5' Tetramethylbenzidine
TPM	Transcripts per million
VST	Variance-stabilizing transformation

Supplementary Information

The online version contains supplementary material available at https://doi.org/10.1186/s13073-026-01677-z.

Additional file 1: Table S1. List of ISGs used for ISG score calculation.

Additional file 2: Table S2. Summary of patient-specific ISG scores for type I, type II, and antiviral ISGs.

Additional file 3: Fig. S1. Transcriptomic levels of detectable type I, type II, and type III IFN mRNA expression across different clinical groups. Fig. S2. PCA plot of whole-blood transcriptomic data, illustrating the clustering of study participants based on ISG-defined groups. Fig. S3. Independent transcriptomic datasets confirm heterogeneous ISG states across COVID-19 cohorts. Fig. S4. Inferred proportions of selected immune cell types across study groups. Fig. S5. Flow cytometry analysis of myeloid cell populations across ISG-defined clusters. Fig. S6. Plasma levels of inflammatory and neutrophil activation markers across disease conditions. Fig. S7. Correlation between metabolite levels and immune activation markers in the HIS cluster. Fig. S8. Western blot analysis of PBMCs from healthy, convalescent, mild and severe patient groups. Fig. S9. Distinct systemic molecular states among clinically severe COVID-19 patients across ISG-defined endotypes. Fig. S10. Sex-associated comparison of systemic ISG expression.

Additional file 4: Table S3. Plasma levels of IFNs measured using LEGENDplex assay.

Additional file 5: Table S4. Differentially expressed plasma proteins across ISG-defined clusters.

Additional file 6: Table S5. List of significantly altered metabolites in ISG-defined clusters.

Additional file 7: Table S6. Correlation of ISG scores with significantly altered metabolites.

Additional file 8: Table S7. Digital cell quantification results for immune cell fractions across ISG clusters.

Additional file 9: Table S8. Plasma levels of S100A8/A9 and neopterin in ISG-defined clusters.

Additional file 10: Table S9. Correlation of ISG scores with immune cell proportions.

Additional file 11: Table S10. Differentially expressed inflammatory mediators in HIS patients with mild vs. severe disease.

Additional file 12: Table S11. Significantly altered metabolites in HIS patients with mild vs. severe disease.

Additional file 13: Table S12. Correlation of metabolic alterations with immune activation markers.

Acknowledgements

The authors would like to thank the excellent support received from the study nurses Elisabet Storgard and Ronnie Ask, Södersjukhuset. We thank the National Facility for Autoimmunity and Serology Profiling at SciLifeLab for excellent technical support related to the antibody-reactivity screening

experiments. We also acknowledge Magdalini Lourda, Karolinska Institutet for meaningful discussions that contributed to this work.

Authors' contributions

SG conceptualized the project; SG, UN, NL and RL-J, acquired the funding; RL-J, AC, SR, AY, SSA, XC, MS and MA-G, performed research; AA and FM, performed bioinformatic analaysis; HN and CJT performed clinical research. NL and UN contributed new reagents/analytic tools; AA, RL-J, SR, AC, AY, FM, SSA, NL, UN and SG analyzed data; SR, AA, AY, RL-J, AC, FM, SSA and SG wrote the original draft of the paper. AC, RL-J, SR, XC, MS, HN, CJT, NL and UN reviewed and edited the manuscript. All authors have reviewed and approved of the final version.

Funding

Open access funding provided by Karolinska Institute. This work was supported by the Swedish Research Council grants 2021–03035 (SG), 2021–00993 (UN), 2018–06156 (UN), and Center for Medical Innovation grant CIMED-FoUI093304 (SG), and received support from Karolinska Institutet Stiftelser och Fonder grant 2022–02232 (SG). NL acknowledges funding from Swedish Research Council and Göran Gustafsson Foundation, and RL-J received support from SOF/Stockholm County Council (FoUI-966258).

Data availability

The datasets analyzed in this study are publicly available from previously published sources. The primary transcriptomic dataset used for reanalysis originates from Ambikan et al. [18] and is available in the Sequence Read Archive (SRA) under accession PRJNA828431 (https://www.ncbi.nlm.nih.gov/sra/PRJNA828431) and through the original publication. Additional multi-omics data were obtained from Krishnan et al. [19]. The metabolomics dataset is available at Figshare (https://dx.doi.org/10.6084/m9.figshare.13336862), and the untargeted quantitative proteomics dataset is available via the ProteomeXchange Consortium through the PRIDE partner repository under accession PXD023760 (https://www.ebi.ac.uk/pride/archive/projects/PXD023760). Publicly available transcriptomic datasets used for independent validation analyses include: Overmyer et al. [30], Gene Expression Omnibus GSE157103 (https://www.ncbi.nlm.nih.gov/geo/query/acc.cgi?acc=GSE157103); Carapito et al. [31], Gene Expression Omnibus GSE172114 (https://www.ncbi.nlm.nih.gov/geo/query/acc.cgi?acc=GSE172114); Stephenson et al. [32], ArrayExpress E-MTAB-10026 (https://www.ebi.ac.uk/arrayexpress/experiments/E-MTAB-10026); and Zhang et al. [33], Genome Sequence Archive, National Genomics Data Center HRA000150 (https://ngdc.cncb.ac.cn/gsa-human/browse/HRA000150). All scripts used for ISG scoring, clustering, and downstream analyses performed in this study are publicly available at: https://github.com/SystemsVirology/ISG_Endotype Processed data supporting the analyses presented in this study are provided within the article and its Supplementary Information files.

Declarations

Ethics approval and consent to participate

The study was approved by the Swedish Ethical Review Authority (Dnr 2020–01865). All individuals gave informed consent, and the study was conducted according to the Declaration of Helsinki.

Consent for publication

Not applicable.

Competing interests

The authors declare no competing interests.

Author details

[1]Division of Oral Diagnostics & Surgery, Department of Dental Medicine, Karolinska Institutet, Huddinge, Sweden
[2]The Systems Virology Laboratory, Division of Clinical Microbiology, Department of Laboratory Medicine, ANA Futura, Karolinska Institutet, Stockholm 141 52, Sweden
[3]Science for Life Laboratory, Department of Medical Biochemistry and Microbiology, Uppsala University, Uppsala, Sweden
[4]Centre for Molecular Medicine, Department of Medicine (Solna), Karolinska Institutet, Stockholm, Sweden
[5]Department of Infectious Diseases/Venhälsan, South General Hospital, Stockholm, Sweden
[6]Department of Medicine Huddinge, Division of Infectious Diseases, Karolinska Institutet, I73, Karolinska University Hospital, Huddinge, Stockholm 141 86, Sweden

Received: 23 March 2025 / Accepted: 20 May 2026
Published online: 29 May 2026

References

1. Parasher A. COVID-19: current understanding of its pathophysiology, clinical presentation and treatment. Postgrad Med J. 2021;97(1147):312–20.
2. Fara A, Mitrev Z, Rosalia RA, Assas BM. Cytokine storm and COVID-19: a chronicle of pro-inflammatory cytokines. Open Biol. 2020;10(9):200160.
3. Swiecki M, Colonna M. Type I interferons: diversity of sources, production pathways and effects on immune responses. Curr Opin Virol. 2011;1(6):463–75.
4. Kim YM, Shin EC. Type I and III interferon responses in SARS-CoV-2 infection. Exp Mol Med. 2021;53(5):750–60.
5. Pervolaraki K, Rastgou Talemi S, Albrecht D, Bormann F, Bamford C, Mendoza JL, et al. Differential induction of interferon stimulated genes between type I and type III interferons is independent of interferon receptor abundance. PLoS Pathog. 2018;14(11):e1007420.
6. Park A, Iwasaki A. Type I and Type III interferons - induction, signaling, evasion, and application to combat COVID-19. Cell Host Microbe. 2020;27(6):870–8.
7. Decker T. The early interferon catches the SARS-CoV-2. J Exp Med. 2021;218(10):e20211667.
8. Zhang Q, Bastard P, Liu Z, Le Pen J, Moncada-Velez M, Chen J, Ogishi M, Sabli IKD, Hodeib S, Korol C, et al. Inborn errors of type I IFN immunity in patients with life-threatening COVID-19. Science. 2020;370(6515):eabd4570.
9. Bastard P, Rosen LB, Zhang Q, Michailidis E, Hoffmann HH, Zhang Y, Dorgham K, Philippot Q, Rosain J, Béziat V, et al. Autoantibodies against type I IFNs in patients with life-threatening COVID-19. Science. 2020;370(6515):eabd4585.
10. Smith N, Possémé C, Bondet V, Sugrue J, Townsend L, Charbit B, et al. Defective activation and regulation of type I interferon immunity is associated with increasing COVID-19 severity. Nat Commun. 2022;13(1):7254.
11. Zhu L, Yang P, Zhao Y, Zhuang Z, Wang Z, Song R, Zhang J, Liu C, Gao Q, Xu Q, et al. Single-Cell Sequencing of Peripheral Mononuclear Cells Reveals Distinct Immune Response Landscapes of COVID-19 and Influenza Patients. Immunity. 2020;53(3):685–696 e683.
12. Acharya D, Liu G, Gack MU. Dysregulation of type I interferon responses in COVID-19. Nat Rev Immunol. 2020;20(7):397–8.
13. Fritsch SD, Weichhart T. Effects of interferons and viruses on metabolism. Front Immunol. 2016;7:630.
14. Crow MK, Ronnblom L. Type I interferons in host defence and inflammatory diseases. Lupus Sci Med. 2019;6(1):e000336.
15. Wang X, Tang Q, Li H, Jiang H, Xu J, Bergquist R, et al. Autoantibodies against type I interferons in COVID-19 infection: a systematic review and meta-analysis. Int J Infect Dis. 2023;130:147–52.
16. Peluso MJ, Deeks SG. Mechanisms of long COVID and the path toward therapeutics. Cell. 2024;187(20):5500–29.
17. Chen Y, Lin Q, Cheng H, Xiang Q, Zhou W, Wu J, et al. Immunometabolic shifts in autoimmune disease: mechanisms and pathophysiological implications. Autoimmun Rev. 2025;24(3):103738.
18. Ambikan AT, Yang H, Krishnan S, Svensson Akusjärvi S, Gupta S, Lourda M, Sperk M, Arif M, Zhang C, Nordqvist H, et al. Multi-omics personalized network analyses highlight progressive disruption of central metabolism associated with COVID-19 severity. Cell Syst. 2022;13(8):665–681 e664.
19. Krishnan S, Nordqvist H, Ambikan AT, Gupta S, Sperk M, Svensson-Akusjärvi S, et al. Metabolic perturbation associated with COVID-19 disease severity and SARS-CoV-2 replication. Mol Cell Proteomics. 2021;20:100159.
20. Vedder D, Gerritsen M, Nurmohamed MT, van Vollenhoven RF, Lood C. A neutrophil signature is strongly associated with increased cardiovascular risk in gout. Rheumatology (Oxford). 2021;60(6):2783–90.
21. Zuo Y, Yalavarthi S, Shi H, Gockman K, Zuo M, Madison JA, Blair C, Weber A, Barnes BJ, Egeblad M, et al. Neutrophil extracellular traps in COVID-19. JCI insight. 2020;5(11):e138999.
22. Le Voyer T, Parent AV, Liu X, Cederholm A, Gervais A, Rosain J, et al. Autoantibodies against type I IFNs in humans with alternative NF-κB pathway deficiency. Nature. 2023;623(7988):803–13.

23. Arrestier R, Bastard P, Belmondo T, Voiriot G, Urbina T, Luyt CE, et al. Autoantibodies against type I IFNs in > 10% of critically ill COVID-19 patients: a prospective multicentre study. Ann Intensive Care. 2022;12(1):121.
24. Love MI, Huber W, Anders S. Moderated estimation of fold change and dispersion for RNA-seq data with DESeq2. Genome Biol. 2014;15(12):550.
25. Carrau L, Frere JJ, Golynker I, Fajardo A, Rivera CF, Horiuchi S, et al. Delayed engagement of host defenses enables SARS-CoV-2 viremia and productive infection of distal organs in the hamster model of COVID-19. Science signaling. 2023;16(789):eadg5470.
26. Ritchie ME, Phipson B, Wu D, Hu Y, Law CW, Shi W, et al. Limma powers differential expression analyses for RNA-sequencing and microarray studies. Nucleic Acids Res. 2015;43(7):e47.
27. Risso D, Ngai J, Speed TP, Dudoit S. Normalization of RNA-seq data using factor analysis of control genes or samples. Nat Biotechnol. 2014;32(9):896–902.
28. Racle J, Gfeller D. EPIC: a tool to estimate the proportions of different cell types from bulk gene expression data. Methods Mol Biol. 2020;2120:233–48.
29. Uhlen M, Karlsson MJ, Zhong W, Tebani A, Pou C, Mikes J, Lakshmikanth T, Forsström B, Edfors F, Odeberg J, et al. A genome-wide transcriptomic analysis of protein-coding genes in human blood cells. Science. 2019;366(6472):eaax9198.
30. Wilkerson MD, Hayes DN. ConsensusClusterPlus: a class discovery tool with confidence assessments and item tracking. Bioinformatics. 2010;26(12):1572–3.
31. Overmyer KA, Shishkova E, Miller IJ, Balnis J, Bernstein MN, Peters-Clarke TM, Meyer JG, Quan Q, Muehlbauer LK, Trujillo EA, et al. Large-Scale Multi-omic Analysis of COVID-19 Severity. Cell Syst. 2021;12(1):23–40 e27.
32. Carapito R, Li R, Helms J, Carapito C, Gujja S, Rolli V, et al. Identification of driver genes for critical forms of COVID-19 in a deeply phenotyped young patient cohort. Sci Transl Med. 2022;14(628):eabj7521.
33. Stephenson E, Reynolds G, Botting RA, Calero-Nieto FJ, Morgan MD, Tuong ZK, et al. Single-cell multi-omics analysis of the immune response in COVID-19. Nat Med. 2021;27(5):904–16.
34. Zhang JY, Wang XM, Xing X, Xu Z, Zhang C, Song JW, et al. Single-cell landscape of immunological responses in patients with COVID-19. Nat Immunol. 2020;21(9):1107–18.
35. Ebrahimi KH, Gilbert-Jaramillo J, James WS, McCullagh JSO. Interferon-stimulated gene products as regulators of central carbon metabolism. FEBS J. 2021;288(12):3715–26.
36. Fletcher M, Ramirez ME, Sierra RA, Raber P, Thevenot P, Al-Khami AA, et al. l-Arginine depletion blunts antitumor T-cell responses by inducing myeloid-derived suppressor cells. Cancer Res. 2015;75(2):275–83.
37. Seo SK, Kwon B. Immune regulation through tryptophan metabolism. Exp Mol Med. 2023;55(7):1371–9.
38. Apel F, Andreeva L, Knackstedt LS, Streeck R, Frese CK, Goosmann C, Hopfner KP, Zychlinsky A. The cytosolic DNA sensor cGAS recognizes neutrophil extracellular traps. Sci Signal. 2021;14(673):eaax7942.
39. Tsou CL, Peters W, Si Y, Slaymaker S, Aslanian AM, Weisberg SP, et al. Critical roles for CCR2 and MCP-3 in monocyte mobilization from bone marrow and recruitment to inflammatory sites. J Clin Invest. 2007;117(4):902–9.
40. Perreau M, Suffiotti M, Marques-Vidal P, Wiedemann A, Levy Y, Laouénan C, et al. The cytokines HGF and CXCL13 predict the severity and the mortality in COVID-19 patients. Nat Commun. 2021;12(1):4888.
41. Hafez W, Nasa P, Khairy A, Jose M, Abdelshakour M, Ahmed S, et al. Interleukin-6 and the determinants of severe COVID-19: a retrospective cohort study. Medicine (Baltimore). 2023;102(45):e36037.
42. Angajala A, Lim S, Phillips JB, Kim JH, Yates C, You Z, et al. Diverse roles of mitochondria in immune responses: novel insights into immuno-metabolism. Front Immunol. 2018;9:1605.
43. Wallner S, Orsó E, Grandl M, Konovalova T, Liebisch G, Schmitz G. Phosphatidylcholine and phosphatidylethanolamine plasmalogens in lipid loaded human macrophages. PLoS ONE. 2018;13(10):e0205706.
44. da Silva RP, Gonçalves JIB, Zanin RF, Schuch FB, de Souza APD. Circulating Type I interferon levels and COVID-19 severity: a systematic review and meta-analysis. Front Immunol. 2021;12:657363.
45. Knight JS, Caricchio R, Casanova JL, Combes AJ, Diamond B, Fox SE, Hanauer DA, James JA, Kanthi Y, Ladd V, et al. The intersection of COVID-19 and autoimmunity. J Clin Invest. 2021;131(24):e154886.
46. Eskandarian Boroujeni M, Sekrecka A, Antonczyk A, Hassani S, Sekrecki M, Nowicka H, et al. Dysregulated interferon response and immune hyperactivation in severe COVID-19: targeting STATs as a novel therapeutic strategy. Front Immunol. 2022;13:888897.
47. Galbraith MD, Kinning KT, Sullivan KD, Araya P, Smith KP, Granrath RE, Shaw JR, Baxter R, Jordan KR, Russell S, et al. Specialized interferon action in COVID-19. Proc Natl Acad Sci U S A. 2022;119(11):e2116730119.
48. Wilk AJ, Rustagi A, Zhao NQ, Roque J, Martínez-Colón GJ, McKechnie JL, et al. A single-cell atlas of the peripheral immune response in patients with severe COVID-19. Nat Med. 2020;26(7):1070–6.
49. Lee JS, Park S, Jeong HW, Ahn JY, Choi SJ, Lee H, Choi B, Nam SK, Sa M, Kwon JS, et al. Immunophenotyping of COVID-19 and influenza highlights the role of type I interferons in development of severe COVID-19. Sci Immunol. 2020;5(49):eabd1554.
50. Zhou Z, Ren L, Zhang L, Zhong J, Xiao Y, Jia Z, et al. Heightened innate immune responses in the respiratory tract of COVID-19 patients. Cell Host Microbe. 2020;27(6):883-890 e882.
51. Daman AW, Josefowicz SZ. Epigenetic and transcriptional control of interferon-ß. J Exp Med. 2021;218(9):e20210039.
52. Lee JS, Shin EC. The type I interferon response in COVID-19: implications for treatment. Nat Rev Immunol. 2020;20(10):585–6.
53. Galani IE, Rovina N, Lampropoulou V, Triantafyllia V, Manioudaki M, Pavlos E, et al. Untuned antiviral immunity in COVID-19 revealed by temporal type I/III interferon patterns and flu comparison. Nat Immunol. 2021;22(1):32–40.
54. Kisand K, Link M, Wolff AS, Meager A, Tserel L, Org T, et al. Interferon autoantibodies associated with AIRE deficiency decrease the expression of IFN-stimulated genes. Blood. 2008;112(7):2657–66.
55. Bastard P, Gervais A, Le Voyer T, Rosain J, Philippot Q, Manry J, Michailidis E, Hoffmann HH, Eto S, Garcia-Prat M, et al. Autoantibodies neutralizing type I IFNs are present in ~4% of uninfected individuals over 70 years old and account for ~20% of COVID-19 deaths. Sci Immunol. 2021;6(62):eabl4340.
56. Porcelijn L, Schmidt DE, Oldert G, Hofstede-van Egmond S, Kapur R, Zwaginga JJ, et al. Evolution and utility of antiplatelet autoantibody testing in patients with immune thrombocytopenia. Transfus Med Rev. 2020;34(4):258–69.
57. Vazquez SE, Mann SA, Bodansky A, Kung AF, Quandt Z, Ferré EMN, Landegren N, Eriksson D, Bastard P, Zhang SY, et al. Autoantibody discovery across monogenic, acquired, and COVID-19-associated autoimmunity with scalable PhIP-seq. eLife. 2022;11:e78550.
58. Mantovani A, Cassatella MA, Costantini C, Jaillon S. Neutrophils in the activation and regulation of innate and adaptive immunity. Nat Rev Immunol. 2011;11(8):519–31.
59. Xia P, Ji X, Yan L, Lian S, Chen Z, Luo Y. Roles of S100A8, S100A9 and S100A12 in infection, inflammation and immunity. Immunology. 2024;171(3):365–76.
60. Mellett L, Khader SA. S100A8/A9 in COVID-19 pathogenesis: impact on clinical outcomes. Cytokine Growth Factor Rev. 2022;63:90–7.
61. Guo Q, Zhao Y, Li J, Liu J, Yang X, Guo X, et al. Induction of alarmin S100A8/A9 mediates activation of aberrant neutrophils in the pathogenesis of COVID-19. Cell Host Microbe. 2021;29(2):222-235 e224.
62. Chauvin M, Larsen M, Quirant B, Quentric P, Dorgham K, Royer L, et al. Elevated Neopterin levels predict fatal outcome in SARS-CoV-2-infected patients. Front Cell Infect Microbiol. 2021;11:709893.
63. Cho SD, Shin H, Kim S, Kim HJ. Insights on interferon-independent induction of interferon-stimulated genes shaping the lung's response in early SARS-CoV-2 infection. Heliyon. 2023;9(12):e22997.
64. Wang W, Xu L, Su J, Peppelenbosch MP, Pan Q. Transcriptional regulation of antiviral interferon-stimulated genes. Trends Microbiol. 2017;25(7):573–84.
65. Ackermann M, Anders HJ, Bilyy R, Bowlin GL, Daniel C, De Lorenzo R, et al. Patients with COVID-19: in the dark-NETs of neutrophils. Cell Death Differ. 2021;28(11):3125–39.
66. Palmer CS. Innate metabolic responses against viral infections. Nat Metab. 2022;4(10):1245–59.
67. Lai M, De Carli A, Filipponi C, Iacono E, La Rocca V, Lottini G, et al. Lipid balance remodelling by human positive-strand RNA viruses and the contribution of lysosomes. Antiviral Res. 2022;206:105398.
68. Lee M, Lee SY, Bae YS. Functional roles of sphingolipids in immunity and their implication in disease. Exp Mol Med. 2023;55(6):1110–30.
69. Masoodi M, Peschka M, Schmiedel S, Haddad M, Frye M, Maas C, et al. Disturbed lipid and amino acid metabolisms in COVID-19 patients. J Mol Med (Berl). 2022;100(4):555–68.
70. York AG, Williams KJ, Argus JP, Zhou QD, Brar G, Vergnes L, et al. Limiting cholesterol biosynthetic flux spontaneously engages type I IFN signaling. Cell. 2015;163(7):1716–29.
71. Icard P, Lincet H, Wu Z, Coquerel A, Forgez P, Alifano M, et al. The key role of Warburg effect in SARS-CoV-2 replication and associated inflammatory response. Biochimie. 2021;180:169–77.

72. Peace CG, O'Neill LA. The role of itaconate in host defense and inflammation. J Clin Invest. 2022;132(2):e148548.
73. Sánchez-García FJ, Pérez-Hernández CA, Rodríguez-Murillo M, Moreno-Altamirano MMB. The role of tricarboxylic acid cycle metabolites in viral infections. Front Cell Infect Microbiol. 2021;11:725043.
74. Giacomelli A, De Falco T, Oreni L, Pedroli A, Ridolfo AL, Calabro E, et al. Impact of gender on patients hospitalized for SARS-COV-2 infection: a prospective observational study. J Med Virol. 2021;93(7):4597–602.
75. Appunni S, Rubens M, Ramamoorthy V, Saxena A, Doke M, Roy M, et al. Gender differences in hospital outcomes among COVID-19 hospitalizations. South Med J. 2024;117(2):75–9.

Publisher's Note